

# A snapshot attractor view of the advection of inertial particles in the presence of history force

Ksenia Guseva<sup>1,a</sup>, Anton Daitche<sup>1</sup>, and Tamás Tél<sup>2</sup>

<sup>1</sup> Theoretical Physics/Complex Systems, ICBM, University of Oldenburg, 26129 Oldenburg, Germany

<sup>2</sup> Institute for Theoretical Physics and MTA-ELTE Theoretical Physics Research Group, Eötvös University, P.O. Box 32, 1518 Budapest, Hungary

Received 7 February 2017 / Received in final form 21 March 2017  
Published online 21 June 2017

**Abstract.** We analyse the effect of the Basset history force on the sedimentation or rising of inertial particles in a two-dimensional convection flow. We find that the concept of snapshot attractors is useful to understand the extraordinary slow convergence due to long-term memory: an ensemble of particles converges exponentially fast towards a snapshot attractor, and this attractor undergoes a slow drift for long times. We demonstrate for the case of a periodic attractor that the drift of the snapshot attractor can be well characterized both in the space of the fluid and in the velocity space. For the case of quasiperiodic and chaotic dynamics we propose the use of the average settling velocity of the ensemble as a distinctive measure to characterize the snapshot attractor and the time scale separation corresponding to the convergence towards the snapshot attractor and its own slow dynamics.

## 1 Introduction

Recent studies have demonstrated the importance of the history force in the advection of small inertial particles in different flow types (see e.g., [1–9]). An important effect that characterizes the dynamics in the presence of this force is the appearance of extraordinary long, diffusive type, transients [5, 7, 10, 11].

The plethora of possible dynamical behaviors in the cellular flow was explored without the history force in [12] and in the presence of this force in [5] for both bubbles and aerosols. Due to the afore-mentioned slow convergence, it was possible to make only approximate statements about the attractors. Here we concentrate on a few cases only, but carry out long term simulations. We make use of the so-called snapshot attractor approach which enables one to explore a time-scale separation, and identify a short term exponential convergence and a long-term power law behavior.

The paper is organized as follows: we start with the main description of the flow and the equation of motion for inertial particles in Section 2; then a short

<sup>a</sup> e-mail: [ksenia.guseva@uni-oldenburg.de](mailto:ksenia.guseva@uni-oldenburg.de)

overview follows about the concept of snapshot attractors and how it will be applied for this system in Section 3. A detailed analysis of the inertial dynamics with periodic, quasiperiodic, and chaotic attractors is given in Sections 4.1, 4.2, and 4.3, respectively. Conclusive comments follow in Section 5.

## 2 Model

We consider small rigid spherical particles of radius  $r_p$  carried by a fluid of kinematic viscosity  $\nu$ . The trajectories of such particles are evaluated according to the Maxey-Riley equation [13, 14], including the corrections by Auton and coworkers [15]. This equation describes the dimensionless evolution of the particle position  $\mathbf{x}(t)$  and velocity  $\mathbf{v}(t) = d\mathbf{x}/dt$  in a flow field  $\mathbf{u}(\mathbf{x}, t)$  as

$$\frac{d\mathbf{v}}{dt} = A(\mathbf{u} - \mathbf{v}) + AW\mathbf{n} + \frac{3R}{2} \frac{D\mathbf{u}}{Dt} - \sqrt{\frac{9AR}{2\pi}} \int_0^t \frac{d(\mathbf{v}-\mathbf{u})}{\sqrt{t-\tau}} d\tau, \quad (1)$$

where  $\frac{D\mathbf{u}}{Dt} = \frac{\partial\mathbf{u}}{\partial t} + \mathbf{u} \cdot \nabla\mathbf{u}$  represents the full derivative along a fluid element,  $\frac{d\mathbf{u}}{dt} = \frac{\partial\mathbf{u}}{\partial t} + \mathbf{v} \cdot \nabla\mathbf{u}$  the derivative along a particle trajectory, and  $\mathbf{n}$  is a unit vector pointing upwards. The last term of this equation represents the Basset history force, the consequences of which will be discussed in this paper. The form (1) implies that the initial velocity of the particles coincides with that of the flow:  $\mathbf{v}(0) = \mathbf{u}(\mathbf{x}_0, 0)$ , what we shall assume throughout the paper.

The parameters of the Maxey-Riley equation are: the inertial parameter

$$A = R \frac{9\nu}{2r_p^2} \frac{L}{U}, \quad (2)$$

where  $L$  and  $U$  are the characteristic size and velocity of the flow (the reciprocal of  $A$  is called the Stokes number), the dimensionless settling velocity in a fluid at rest

$$W = \frac{gL}{U^2} \frac{R}{A} \left( \frac{3}{2} - \frac{1}{R} \right), \quad (3)$$

with  $g$  as the gravitational acceleration, and the density ratio

$$R = \frac{2\rho_f}{\rho_f + 2\rho_p} \quad (4)$$

where  $\rho_p$  and  $\rho_f$  stand for the particle and fluid density, respectively. The value of  $R$  divides the particles into aerosols ( $R < 2/3$ ) and bubbles ( $R > 2/3$ ), and relation (3) expresses the fact that aerosols tend to sediment ( $W < 0$ ) and bubbles to rise ( $W > 0$ ).

The velocity field  $\mathbf{u}(\mathbf{x}, t)$  is chosen to be a paradigmatic two-dimensional model of a convective cell flow, introduced in [16] in its time independent form. It consists of oscillating cellular vortices in the plane  $(x, y)$ , where  $y$  is the vertical coordinate increasing upwards. Taking  $L$  and  $U$  in (2) as a characteristic size and the maximal velocity within one vortex, respectively, the dimensionless velocity field is written as

$$\mathbf{u}(\mathbf{x}, t) = (1 + k \sin \omega t) \begin{pmatrix} \sin(\pi x) \cos(\pi y) \\ -\cos(\pi x) \sin(\pi y) \end{pmatrix}. \quad (5)$$

The flow is doubly periodic in both directions with a dimensionless spatial period of 2. We define the unit square containing a single vortex as a box, and the two-by-two square of four vortices as a cell (with two vortices in the horizontal and

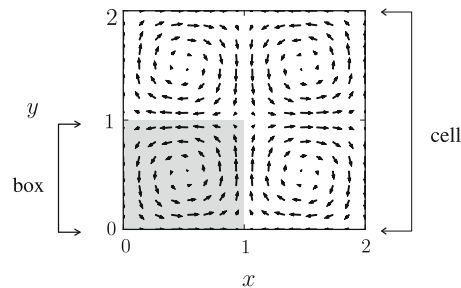


**Fig. 1.** Velocity field at time  $t = 0$ , represented by small arrows, in the elementary cell, the cell containing the origin. The left lower box is shaded to indicate that the initial conditions of Section 4 will be taken from this box.

two in the vertical directions), see Figure 1. Each vortex is rotating in the opposite direction of its four neighbours, and is subjected to a periodic forcing of dimensionless period  $T = 2\pi/\omega$ . The flow parameters are chosen traditionally as  $k = 2.72$  and  $\omega = \pi$  [17–19], i.e., the dimensionless period is  $T = 2$ .

The integration of equation (1) has been performed by a special algorithm which handles the history force appropriately. The details are described in [5], where an adapted version of the algorithm presented in [4] was implemented.

### 3 The snapshot attractor view

In the classical view based on single trajectories, we concluded in [5] that the attractor can be reached after a very long time only. There is, however, an alternative view, that of particle *ensembles*, also available. In autonomous systems the two views are equivalent, which is not so obvious in non-autonomous problems, like the Maxey-Riley equation (1). In this class, one defines a snapshot attractor [20] as an object that attracts all the trajectories initialized in the remote past. It can be obtained by monitoring an ensemble of particle trajectories all subject to the same non-autonomous equation of motion, the members of which do not interact with each other. After a characteristic dissipative time, the ensemble traces out a snapshot attractor. This attractor might, however, move continuously in time. The concept is known for many years (see e.g., [21, 22]), found recent applications in climate dynamics [23–25] and the ensemble concept also motivates a novel type of experimental approach [26, 27]. If the driving is persistent, the snapshot attractor is typically a fractal-looking object whose shape is evolving in time. With vanishing driving, however, the snapshot attractor might be nonchaotic and have a time-dependence that ceases asymptotically [28–30].

In our problem when bubbles rise they often become captured by one of the vortices. In such cases a slow convergence towards a traditional periodic attractor takes place. One can then assume that close to this attractor the effect of the history force for neighboring members of the particle ensemble can locally be considered as a non-autonomous perturbation superimposed on the usual memoryless inertial particle dynamics. An ensemble of particles might then converge to a snapshot attractor, a fixed point on the stroboscopic map, after some time. This snapshot fixed point attractor is then slowly drifting towards the asymptotic traditional attractor. Here a separation of time scales is expected to occur since the convergence to the snapshot attractor is a usual dissipative effect, and hence this decay should be exponential, whereas the slow drift is due to the diffusive Basset kernel, and this leads to a long-term power-law dependence of the location of the fixed point-type snapshot attractor.

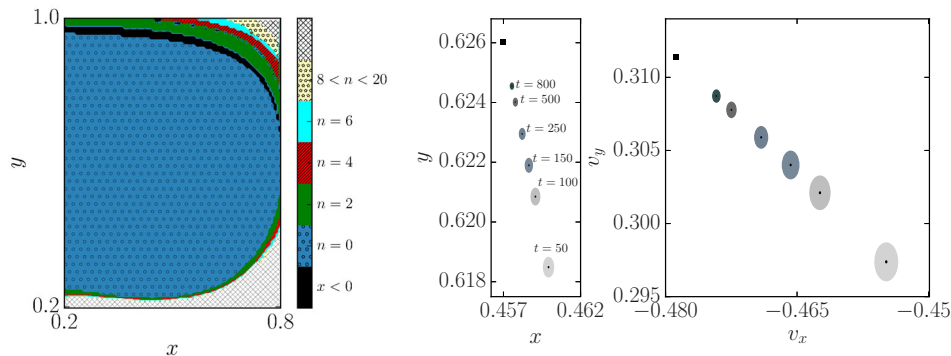


**Fig. 2.** Left panel: basins of attraction of different attractors on the plane of initial conditions. Different shades (colors) indicate the periodic attractors located at  $n$  units (boxes) higher. The basin of permanent rising is marked as cross hatched area. In black we indicate particles that move horizontally across the border to the next box at the left and become captured there. Central and right panels: the time evolution of the center of mass (black dots) of the  $n = 0$  ensemble surrounded by a colored disc of the radius of the standard deviation in the configuration and in the velocity space, respectively. Time is given in units of the period  $T$ . Isolated squares represent the traditional fixed point attractor.

This can be shown by plotting the average distance of the ensemble from the asymptotic fixed point attractor on a stroboscopic map taken with the period  $T$ , in which after an exponential initial decay an asymptotic power law approach can be observed. This behavior was pointed out in [7] for open flows, our study generalizes thus this approach to spatially periodic or closed flows.

Quasiperiodic or chaotic asymptotic attractors are typical in our problem for the sedimentation dynamic of aerosols, where the presence of gravity introduces new aspects for the dynamics. Although a change of the snapshot attractor can also be observed in these cases, the distance of the ensemble from the asymptotic attractor is hardly possible to determine. We have found that a physically interesting quantity of the snapshot attractor is the average settling velocity taken over the ensemble at any instant of time. It is in this average (as well as in other averages or standard deviations) in which a short term exponential decay can be identified, followed by a long-term  $t^{-1/2}$  decay. This observation supports that the phase of exponential decay can be identified with the convergence towards a (quasiperiodic or chaotic) snapshot attractor. This attractor exhibits a long-term power law drift towards an asymptotic traditional attractor.

## 4 Results

### 4.1 Periodic attractor

First we consider bubbles with parameters  $R = 1$ ,  $A = 5$ ,  $W = 0.5$ . Initially  $N = 10800$  such particles are homogeneously distributed in a large portion of the left lower box of the elementary cell shown in Figure 2. Since light particles are typically attracted towards vortex centers, the advection dynamics even in the presence of the history force brings a considerable amount of these particles towards the central region of this same box, where a periodic attractor is located. A smaller portion of the ensemble, nevertheless, leaves the box of initialization and moves to the left or upwards. In Figure 2 we represent with different colors the initial conditions that

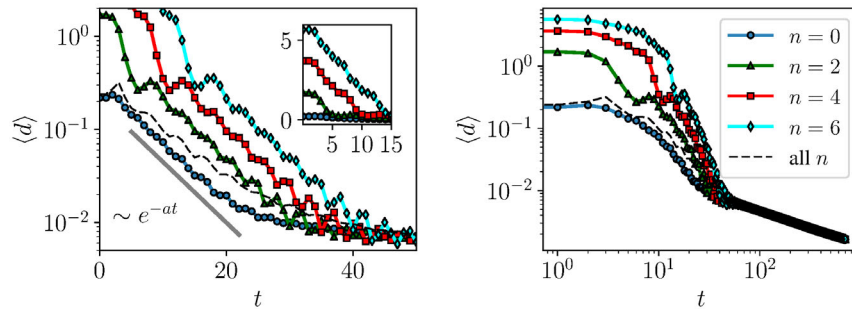


**Fig. 3.** Average distance of selected ensembles of particles to the usual attractors located at  $(x_n^*, y_n^*)$  as a function of time. The fitted decay exponent is  $a = 0.15$ . The dashed curve shows the time dependence of the average distance in periodic representation (see text).

correspond to attractors in different boxes. The initial conditions of particles that move to the neighboring box on the left ( $-1 < x < 0$ ) and are captured there are indicated with black. Particles that move upwards might be trapped in one of the next cells, always in the lower left box of the cell, i.e., an even number of boxes above the box of initialization. The basins of attraction of these periodic attractors are indicated with different colors (shades) in Figure 2. Initial condition belonging to a permanent rising upwards are indicated by the cross hatched area.

As a first attempt of the snapshot approach, we consider the sets of particles that remain in the original box:  $n = 0$ , and those who are captured  $n = 2, 4$  or  $6$  boxes higher. The size of these ensembles are  $N_0 = 5225$ , and  $N_2 = 444, N_4 = 136$  and  $N_6 = 66$ , respectively. On a stroboscopic map taken at integer multiples of  $T$ , the periodic traditional attractors are found by following *single trajectories* up to time about  $t = 10^4 T$  to lie at  $(x_n^*, y_n^*) = (0.45696165, 0.62604046 + n)$ . We evaluated the average distance of the *ensembles*  $n = 0, \dots, 6$  from the corresponding traditional attractors, i.e., the quantities  $\langle d \rangle = 1/N_n \sum_{i=0}^{N_n} \sqrt{(x_i(t) - x_n^*)^2 + (y_i(t) - y_n^*)^2}$ , where  $i$  indicates the index of the particles in the ensemble. The results for the functions  $\langle d \rangle$  vs  $t$  are shown in Figure 3 both in a log-lin representation (left panel) and in a log-log representation. Here and in all the figures of the paper time is measured in units of  $T$ , of the period of the flow. The left panel shows that after some transients an exponential decay sets in for about 20 periods with the same slope  $-0.15$  in all cases. The inset is in lin-lin representation and indicates that before being captured at a box, the rise is approximately linear, and the exponential approach starts only after the box of final destination has been reached. This exponential phase we attribute to the approach to a periodic snapshot attractor as such approach to attractors is typical in dissipative systems. The right panel indicates that after about  $80T$  all ensembles exhibit a  $t^{-1/2}$  convergence towards  $(x_n^*, y_n^*)$ . The size of the ensembles is by this time very small (less than  $10^{-3}$ , see Fig. 4), thus the time dependence in this phase arises from a slow drift of the fixed point snapshot attractor to the traditional asymptotic fixed point attractor. This drift is illustrated by the two right panels of Figure 2 where the location of the center of mass, i.e., of the fixed point snapshot attractor of the  $n = 0$  ensemble is plotted as a function of time both in space and velocity. The radius of the disc about these points is set by the standard deviation of these ensembles. The fact that their values are negligibly small on the scale of the flow (of a box) supports the view that these attractors can be considered fixed point attractors. One sees in the right panels of Figure 2 that the fixed point snapshot attractor still moves after  $500T$  and has yet to reach the traditional attractor represented by the isolated black squares.

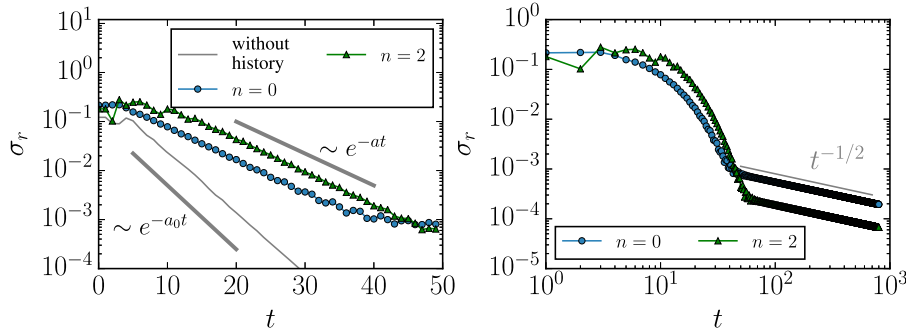


**Fig. 4.** Standard deviation of the ensemble of particles  $\sigma_r = \sqrt{\langle x^2 \rangle - \langle x \rangle^2 + \langle y^2 \rangle - \langle y \rangle^2}$  for ensembles  $n = 0$  and  $n = 2$  as a function of time. The fitted decay exponent is  $a = 0.15$ . The gray line in the left panel represents the same for the  $n = 0$  ensemble in the memoryless dynamics, i.e., by neglecting the history force, and decays with an exponent  $a_0 = 0.3$ .

The dashed curve in Figure 3 is obtained as the average distance of all the particles from the single traditional attractors in periodic representation, i.e., after shifting all coordinates back vertically into the original box whenever the elementary cell is left. While the power law behavior is exactly the same as in the individual ensembles, there is no straight line behavior in the left panel. We thus conclude that a periodic representation of these data would not indicate the exponential behavior since it sets in after different transients in the ensembles of different  $n$  values. Therefore the curve resulting in the periodic representation is bent.

To make the picture more complete, we evaluated the standard deviations in the configuration space of the ensembles at any instant of time, which correspond to the average size of the ensemble in the flow. These quantities are conceptually different from the distances used above since they are independent of the location of the traditional attractor, and are thus also easier to determine. The results for the two largest ensembles  $n = 0$  and  $n = 2$  are plotted in Figure 4. The left panel shows again an exponential decay up to about  $40T$  with the same slope  $-0.15$  for both ensembles. Here we also indicated the size of the  $n = 0$  ensemble *without* the history force (gray line) whose decay is exponential, too, but much faster, of the slope  $(-0.30)$ . This clearly illustrates that the history force makes the dynamics less dissipative than the memoryless dynamics, as observed by several authors (see e.g., [1, 3, 7, 10]). We note that the standard deviation in the velocity space (not shown) reveals the same decay rates as those in the left panel of Figure 4, followed by a  $t^{-1/2}$  asymptotics.

## 4.2 Quasiperiodic attractor

To study quasiperiodic attractors we chose the case of aerosol particles with parameters  $R = 0.5$ ,  $A = 5$ ,  $W = -0.5$ . We note that there are also parameters where the dynamics of bubbles are governed by quasiperiodic attractors, however this type of motion is more typical for sedimentation. Aerosols with these parameters fall through all the cells and their motion is governed by four different quasiperiodic attractors, depending on the initial condition. We illustrate the approach to two traditional attractors in Figure 5. In fact, using the moral learned in the periodic case, we take snapshot attractors which are assumed to be close to the traditional ones after long times, here at  $t = 1000T$ . Remember that the distance between the traditional and the snapshot fixed point attractors at this time was on the order  $2 \times 10^{-3}$  in Figure 3.

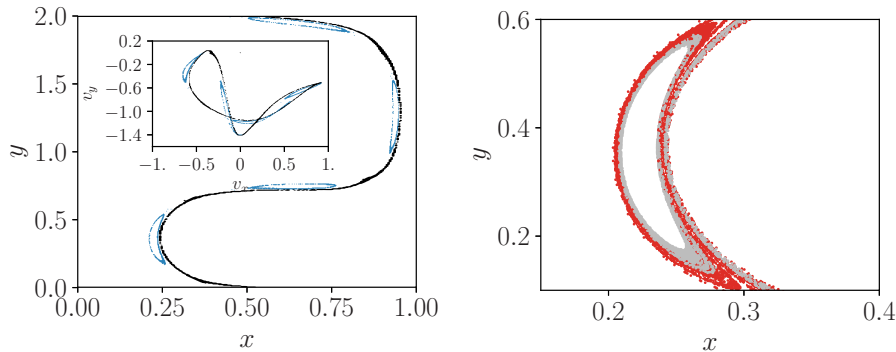


**Fig. 5.** Left: two quasiperiodic snapshot attractors (one marked in black and the other one in blue/grey) after  $1000T$  on the stroboscopic map in periodic representation. The inset shows both attractors in the velocity space. Right: the shape of the ensembles at earlier times: red/dark grey dots at  $300T$ , light grey dots at  $500T$ . For these plots we took an ensemble of  $N = 10^4$  particles initialized within a square:  $x \in [0.33, 0.66]$  vs.  $y \in [0.33, 0.66]$ , uniformly distributed. The ensembles are then split into two according to the coloring in the left panel.

For simplicity, a periodic representation of the snapshot attractors is used here, i.e., the points of any trajectory on the stroboscopic map are shifted back to the elementary cell, the left half of which is shown in the figure. An ensemble of  $N = 10^4$  points is initiated in the middle of this region. At  $1000T$  one sees that the points can be grouped in two disjoint sets, two snapshot attractors exist. The one consisting of loops is marked in blue/grey, the other one in black. The right panel illustrates how this pattern evolves in time.

The larger pattern (red/dark grey) belonging to the earlier time instant appears to trace out a loop and an arch which are connected. In the smaller pattern (light grey) of a later time instant, the loop and the arch are detached (their shape slightly differs from the red ones and both are thinner than in red/dark grey). This indicates that the single snapshot attractor bifurcates into two disjoint ones at about  $500T$ .

The time evolution of the snapshot attractor can be quantified in a compact way by following any averaged quantity taken over the ensemble as a function of time. In the context of sedimentation, perhaps the most natural choice is the average vertical velocity  $\langle v_y \rangle$ . We evaluated this average over both attractors and found a very slow convergence towards a constant terminal velocity (which are slightly different on the two attractors). In Figure 6 we show the results for the black ensemble only. The left upper panel shows  $\langle v_y \rangle$  on the stroboscopic map as a function of time. The fact that an oscillatory behavior appears here to be superimposed on a smooth dependence is a clear sign of the quasiperiodic nature of the problem: besides  $T$ , other frequencies are also present in the dynamics. In spite of the fluctuations, one sees a fast first increase in the average falling speed up to about  $50T$ . After this, a plateau is formed on which a slow convergence to a constant occurs. As a first approximation to the terminal settling velocity  $W^*$  we take the last value of  $\langle v_y \rangle$ ,  $\langle v_y \rangle(1000T) = -0.7258$ . Plotting the difference  $\langle v_y \rangle - W^*$  as a function of time on a log-log plot, an asymptotic straight line of slope  $-1/2$  can be observed, similar to what is visible in the right panel. By slightly changing the value of  $W^*$ , it was possible to find in some cases a better fit to a straight line. In a self-consistent way, we considered the  $W^*$  value to be the true terminal velocity which provides the best long term power law fit to the difference, and this is plotted in the right panel. The left lower panel shows the same quantity on a log-lin representation and reveals an exponential decay of slope  $-0.075$ .

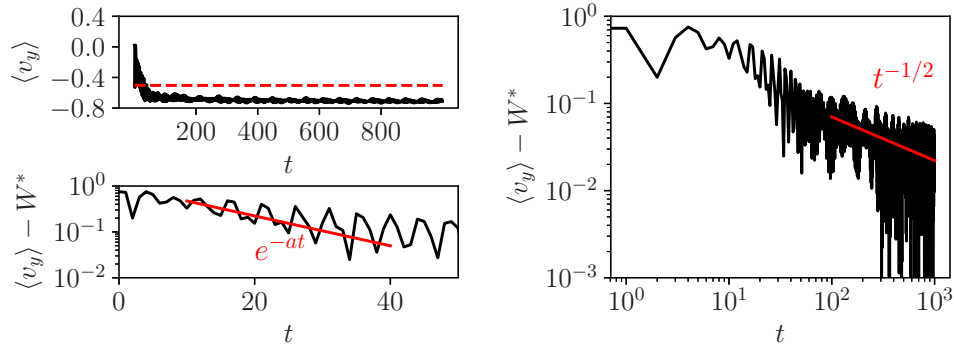


**Fig. 6.** Convergence towards a terminal velocity on the attractor marked in black in Figure 5, represented by an ensemble of 2582 particles from the total ensemble. Left upper panel:  $\langle v_y \rangle$  vs time. Dashed red line represents the value of  $W$  taken in (1). The terminal velocity is thus faster in our flow than in a fluid at rest. Right panel: the quantity  $\ln(\langle v_y \rangle - W^*)$  vs.  $\ln t$  with  $W^* = -0.732$ . Left lower panel:  $\ln(\langle v_y \rangle - W^*)$  vs.  $t$  and a linear fit of slope  $a = 0.075$  over the range  $10 - 40T$ .

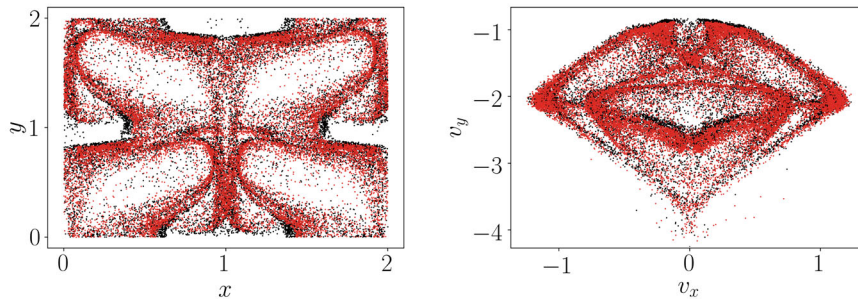


**Fig. 7.** Snapshot chaotic attractors on the stroboscopic map in periodic representation in time window  $[100T, 110T]$  in black, overlaid with the ones from the window  $[990T, 1000T]$  in red/dark grey.

### 4.3 Chaotic attractor

As a last example we take aerosols with parameters:  $R = 0.5$ ,  $A = 1.27$ ,  $W = -2.05$ . In this case a single asymptotic chaotic attractor governs the sedimentation. We start with an ensemble of  $N = 3600$  particles initialized in the left lower corner of the cell:  $x \in [0, 0.66]$ ,  $y \in [0, 0.66]$ . In this system, additionally to the chaotic attractor, there is a regular attractor which corresponds to particles falling at the division between cells, i.e., along the vertical line  $x = 0, x = 2$ . All particles that converge to this simple attractor are carefully eliminated, thus we discuss quantities attributed only to particles advected chaotically.

Figure 7 exhibits the snapshot attractor on the stroboscopic map, the instantaneous pattern traced out by the ensemble, in a time window about  $t = 100T$  in black, superimposed on this with red/grey the snapshot attractor in a time window about  $t = 1000T$ . Both patterns are fractal like, but differ from each other, i.e., the snapshot chaotic attractor is also changing in time.

The ensemble average of the settling velocity  $\langle v_y \rangle$  changes similarly as in the left panel of Figure 6, therefore we do not show this graph here. The only difference is that the settling velocity with such particles is smaller in this cellular flow than in a

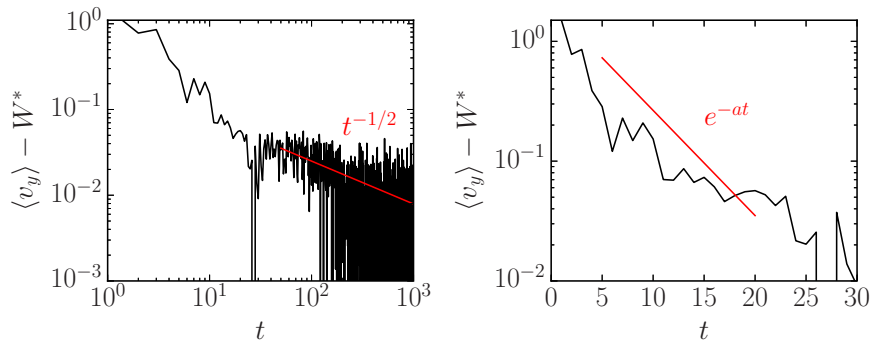


**Fig. 8.** Convergence towards a terminal velocity on the chaotic attractor represented by an ensemble of size  $N = 2700$ . Left: log-log and right: log-lin plot of  $\langle v_y \rangle - W^*$  vs.  $t$  with  $W^* = -1.9479$ ,  $a = 0.2$ . The ensemble was initialized in the square:  $x \in [0, 0.66]$  vs.  $y \in [0, 0.66]$ .

still fluid. In Figure 8 we plot the average settling velocity on the snapshot attractor and its convergence towards a terminal velocity. Here again a long-term power-law decay is found with a fitted terminal velocity  $W^* = -1.9479$  (left panel) preceded by an exponential decay (right panel) of slope  $-0.20$ .

## 5 Conclusion

We have applied the concept of snapshot attractors to interpret the transient dynamics in the advection of inertial particles subjected to gravity in the presence of history force. This approach offers a clear interpretation of the well-known extraordinary slow convergence of single trajectories to attractors by applying an ensemble view. This shows a separation of the dynamics into two phases: a short-term exponential convergence of the particle ensemble towards a snapshot attractor, followed by a very slow drift or deformation of this snapshot attractor both in the space of the fluid and in the full phase space. This latter phase is governed by a power law decay as a consequence of the diffusive nature the history kernel. These two phases can also be observed in any average taken over the ensemble. In the context of sedimentation, a physically relevant ensemble average is that of the settling velocity in which we also find a short-term exponential decay, followed by a  $t^{-1/2}$  convergence towards a constant terminal velocity. Our results imply that stationary statistics of the particle motion with the history force are expected to set in after very long transient periods only. This can be also expected for processes like collisions and aggregation-fragmentation, which are of high importance for environmental phenomena, e.g., in the formation and settling of marine snow [11, 12, 19]. Based on our findings, we claim that also for these processes the snapshot attractor approach is a useful tool for the understanding of the transient non-stationarity of the statistics.

The authors would like to wish Ulrike Feudel a happy birthday!

## References

1. R. Toegel, S. Luther, D. Lohse, Phys. Rev. Lett. **96**, 114301 (2006)
2. J.R. Angilella, Phys. Fluids **19**, 073302 (2007)
3. A. Daitche, T. Tél, Phys. Rev. Lett. **107**, 244501 (2011)

4. A. Daitche, J. Comput. Phys. **254**, 93 (2013)
5. K. Guseva, U. Feudel, T. Tél, Phys. Rev. E **88**, 042909 (2013)
6. S. Olivieri, F. Picano, G. Sardina, D. Iudicone, L. Brandt, Phys. Fluids **26**, 041704 (2014)
7. A. Daitche, T. Tél, New J. Phys. **16**, 073008 (2014)
8. L. Bergougnoux, G. Bouchet, D. Lopez, E. Guazzelli, Phys. Fluids **26**, 093302 (2014)
9. M. Farazmand, G. Haller, Nonlinear. Anal. **22**, 98 (2015)
10. A. Daitche, J. Fluid Mech. **782**, 567 (2015)
11. K. Guseva, A. Daitche, U. Feudel, T. Tél, Phys. Rev. Fluids **1**, 074203 (2016)
12. J. Zahnw, U. Feudel, Phys. Rev. E **77**, 026215 (2008)
13. M.R. Maxey, J.J. Riley. Phys. Fluids **26**, 883 (1983)
14. R.J. Gatignol, Mech. Theor. Appl. **1**, 143 (1983)
15. T.R. Auton, J.C.R. Hunt, M. Prud'Homme, J. Fluid Mech. **197**, 241 (1988)
16. M.R. Maxey, Phys. Fluids **30**, 1915 (1987)
17. T. Nishikawa, Z. Toroczkai, C. Grebogi, T. Tél, Phys. Rev. E **65**, 026216 (2002)
18. J. Zahnw, R.D. Vilela, U. Feudel, T. Tél, Phys. Rev. E **77**, 055311 (2008)
19. J. Zahnw, R.D. Vilela, T. Tél, U. Feudel, Phys. Rev. E **80**, 026311 (2009)
20. R. Romeiras, C. Grebogi, E. Ott, Phys. Rev. A **41**, 784 (1990)
21. J.C. Sommerer, E. Ott, Science **259**, 335 (1993)
22. R. Serquina, Y.-C. Lai, G. Chen, Phys. Rev. E **77**, 026208 (2008)
23. M. Ghil, M.D. Chekroun, E. Simonnet, Physica D **327**, 2111 (2008)
24. T. Bodai, G. Károlyi, T. Tél, Nonlinear Process Geophys. **18**, 573 (2011)
25. M. Herein, G. Drótos, T. Haszpra, J. Márffy, T. Tél, Sci. Rep. **7**, 44529 (2017)
26. M. Vincze, Modeling Climate Change in the Laboratory, in *Teaching Physics Innovatively*, edited by A. Király, T. Tél (PhD School of Physics, Eötvös University, Budapest, 2016), pp. 107–118
27. M. Vincze, I. D. Borcia, U. Harlander, Sci. Rep. **7**, 254 (2017)
28. A. Pikovsky, in *Nonlinear and Turbulent Processes in Physics*, Vol. 3, edited by R.Z. Sagdeev (Harwood Acad. Publ., Reading, 1984), pp. 1601–1604
29. A. Pikovsky, Radiophys. Quantum Electron. **27**, 576 (1984)
30. B. Kaszás, U. Feudel, T. Tél, Phys. Rev. E **94**, 062221 (2016)